Published in final edited form as:
Glia. 2012 April ; 60(4): 541–558. doi:10.1002/glia.22287.

Effects of aging and sensory loss on glial cells in mouse visual and auditory cortices

Marie-Ève Tremblay[1,3,*], **Martha L. Zettel**[1,*], **James R. Ison**[1,2], **Paul D. Allen**[1], and **Ania K. Majewska**[1]

[1]Department of Neurobiology and Anatomy and Center for Visual Science, University of Rochester, 601 Elmwood Ave, Rochester, New York 14642

[2]Department of Brain and Cognitive Science, University of Rochester, Rochester, New York 14627

Abstract

Normal aging is often accompanied by a progressive loss of receptor sensitivity in hearing and vision, whose consequences on cellular function in cortical sensory areas have remained largely unknown. By examining the primary auditory (A1) and visual (V1) cortices in two inbred strains of mice undergoing either age-related loss of audition (C57BL/6J) or vision (CBA/CaJ), we were able to describe cellular and subcellular changes that were associated with normal aging (occurring in A1 and V1 of both strains) or specifically with age-related sensory loss (only in A1 of C57BL/6J or V1 of CBA/CaJ), using immunocytochemical electron microscopy and light microscopy. While the changes were subtle in neurons, glial cells and especially microglia were transformed in aged animals. Microglia became more numerous and irregularly distributed, displayed more variable cell body and process morphologies, occupied smaller territories, and accumulated phagocytic inclusions that often displayed ultrastructural features of synaptic elements. Additionally, evidence of myelination defects were observed, and aged oligodendrocytes became more numerous and were more often encountered in contiguous pairs. Most of these effects were profoundly exacerbated by age-related sensory loss. Together, our results suggest that the age-related alteration of glial cells in sensory cortical areas can be accelerated by activity-driven central mechanisms that result from an age-related loss of peripheral sensitivity. In light of our observations, these age-related changes in sensory function should be considered when investigating cellular, cortical and behavioral functions throughout the lifespan in these commonly used C57BL/6J and CBA/CaJ mouse models.

Keywords

microglia; oligodendrocyte; morphology; phagocytosis; CBA/CaJ; C57BL/6J

Introduction

Normal aging is associated with a decline in neural function thought to be caused by cellular and molecular changes in the brain that are distinct from those associated with neurodegenerative diseases. There is now a consensus that widespread central neuronal loss

Corresponding author: Ania K. Majewska, Ph.D. Ania_Majewska@URMC.rochester.edu; Address: Department of Neurobiology and Anatomy and Center for Visual Science, University of Rochester, 601 Elmwood Ave, Rochester, New York 14642; Telephone: 585-275-4173.
[3]Current address: Department of Psychiatry, University of Wisconsin, 6001 Research Park Blvd, Madison, Wisconsin 53719.
[*]These authors contributed equally.

is not associated with normal aging in animals (Peters 1996; Rapp and Gallagher 1996) and humans (Anderson et al. 1983; Cragg 1975) and that neural dysfunction is likely mediated by a region-specific remodeling of synapses (Burke and Barnes 2006; Hof and Morrison 2004; Uemura 1985). These neuronal alterations, however, may be secondary to the larger age-related changes in glial cells that have been associated with decreased neuroprotective function and increased neurotoxicity (Flanary et al. 2007; Luo et al. 2010; Lynch 2010; Streit et al. 2008; von Bernhardi et al. 2010). In particular, previously described changes in microglia include altered cytokine production (Inamizu et al. 1985; Sheng et al. 1998; Sierra et al. 2007), increased expression of activation markers (Ogura et al. 1994; Perry et al. 1993; Sheffield and Berman 1998), and the emergence of dystrophic morphologies (Streit et al. 2004).

Central changes observed during aging may be compounded by aging-associated diseases and by other events distinct from the normal aging process, such as exposure to toxicants, injury or infections (Bilbo 2010; Zimniak 2008). It is very likely that the deterioration of sensory perception, which is a common complaint in older humans and is often due to the degeneration of the peripheral sensory organs (Congdon et al. 2004; Tobias et al. 1988) may also result in central histopathology. In particular, the loss of either hearing or sight severely impacts the quality of life, thus contributing to social withdrawal, anxiety and depression (Sharts-Hopko 2009; Tobias et al. 1988). Whether such age-related alterations in sensory input influence the aging process within the brain is not well understood, but given the large literature describing plastic changes in neuronal circuits, synapses and glial cells in sensory cortical areas following sensory deprivation (Hensch 2005; Tremblay et al. 2010a), we hypothesized that age-related changes in sensory function could influence the normal process of cortical senescence in a similar manner.

To disentangle the cortical effects of aging and age-related loss of sensory function, we examined two commonly used strains of inbred mice, the C57BL/6J (C57) and CBA/CaJ (CBA), which display similar lifespans (30.6 months versus 28.8 months respectively; Willott et al. 1994) but different patterns of age-related sensory loss. Several experiments measuring auditory evoked potentials have compared hearing loss across the lifespan in these strains (Henry and Chole 1980; Hunter and Willott 1987; Li and Borg 1991; Willott 1986; and including the present research) to show that C57 mice begin to lose their hearing as young adults, while CBA mice maintain their hearing thresholds until near senescence. In contrast, in studies of visual loss the C57 mouse shows the least age-related retinal degeneration (Danciger et al. 2007), and only a modest change in electroretinogram recordings at two years of age (Caruso et al. 2010; Williams and Jacobs 2007). Up to about three months of age the CBA mouse has normal retinal function (Dalke et al. 2004; Clapcote et al. 2005), but in the present study we provide behavioral evidence for an age-related loss of photic sensitivity in this strain.

Together, the comparison of C57 and CBA mice, from early adulthood into senescence, provided a unique opportunity to study brains at the same chronological and biological age, one with age-related reduced auditory input but relatively well maintained visual input, and the other with a converse age-related deficit in visual input. By examining the primary auditory (A1) and visual (V1) cortices of the same C57 and CBA mice using immunocytochemical electron microscopy and light microscopy, we were able to describe changes in neurons, microglia, astrocytes and oligodendrocytes that appeared to be driven by aging or a combination of aging and sensory loss. In particular, microglia were found to change their distribution and morphology during aging, while accumulating phagocytic inclusions that displayed ultrastructural features of synaptic elements. Our results propose a complex relationship between aging and age-related sensory dysfunction (arising from a loss of peripheral sensitivity) in effecting cortical senescence.

Materials and Methods

Animals

Animals were treated in strict accordance with the University of Rochester Committee on Animal Resources and the National Institutes of Health standards. All mice were raised from birth in a separate vivarium facility within the University of Rochester under a 12h/12h dark-light cycle and ambient noise levels of 40 dB (SPL) at 2,000 kHz, dropping off linearly to 25 dB SPL at 24 kHz on a log frequency scale. Both male and female mice were used for this study. There was a total of 257 mice tested in the behavioral experiments, 61 CBA mice and C57 mice in the photic experiment (with 7 CBA mice and 21 C57 mice tested at more than one age), 61 CBA mice and 60 C57 mice in the acoustic experiment (25 CBA mice tested at more than one age), and 599 mice were tested with auditory evoked potentials (302 CBA and 297 C57 mice). The large number of ABR records was available because the hearing ability of all of the mice in our colony was tested with the ABR prior to their entry into other experiments.

Behavioral Testing for Acoustic and Photic Sensitivity: the Inhibition of the Acoustic Startle Response (ASR)

For ASR testing, mice were individually confined to a 7 × 5 × 4 cm stainless steel wire cage located in a 1 × 1 × 1 m anechoic chamber (Eckel Corporation) placed within a sound attenuating room (Industrial Acoustics Company). The cage was mounted on a stiff acrylic shelf just above an attached accelerometer (Statham Laboratories) that was sensitive to the vertical force of the startle flinch response. The output of this transducer was passed through a bridge amplifier and integrated over a 100 ms period that began with the onset of the startle-eliciting stimulus. The startle stimulus was a 110 dB (SPL) noise burst, 25 ms in duration, delivered through a high-frequency speaker (JBL Professional). For a human observer a noise burst at this level and duration approximates the sensation produced by snapping one's middle finger off the thumb into the palm, from a distance of about 6″ from the ear. The noise stimulus was calibrated using a 1/4″ microphone (Bruel & Kjaer) placed at the level of the test cage.

Two test stimuli were used to measure age-related changes in sensitivity to acoustic and photic stimuli. In the photic experiment the prestimulus was a 20 ms flash of light provided by a voltage-regulated fluorescent lamp (Sylvania), which had near instantaneous rise and fall times. The lamp was placed behind a double glazed frosted window in a sound-attenuating box in order to eliminate the slight noise coincident with light onset. The intensity of the light was measured with a Spectra Candela Meter (PhotoResearch Corporation) held at the level of the floor of the test cage. The intensity of the light flash was 20 lux and its duration was 20 ms. In the acoustic experiment the prestimulus was a 10 ms quiet gap (with ~0 ms rise and fall times) in an otherwise continuous 70 dB SPL wide band noise delivered through a Panasonic high-frequency speaker. In both experiments the animals were tested in the dark. In the photic experiment mice were group housed for 30 min in a room illuminated by red light, followed by a 10 min period of dark adaptation in the individual test chamber. The photic experiment consisted of 132 trials, averaging 17 s apart (range 15 to 20), delivered in 11 blocks of 12 trials. The noise burst that elicited the reflex response was presented alone (a baseline control trial, presented twice in each block of 12 trials), or preceded by the light flash, with light-onset to noise-onset lead times of 10, 20, 30, 40, 50, 70, 110, 160, 220 ms, with one additional "no-stimulus trial" to assess background spontaneous activity. In the acoustic experiment the test session consisted of 121 trials, on average 17 s apart, delivered in 11 blocks of 11 trials. Each block included two baseline control trials, 8 trials in which the startle stimulus was preceded by a 10 ms gap in noise, the gap beginning 10, 15, 20, 30, 40, 60, 110 or 160 ms before the startle stimulus, with one

additional "no stimulus" trial. The order of conditions in each block was randomized, and the first block of trials was not used in the data analysis, in part because the startle reflex can be unusually large on the first few trials after confinement in the quiet test cage.

Prepulse inhibition scores were calculated as the ratio of each subject's mean startle response amplitude in the prepulse condition (ASR_p) compared with the no-prepulse control baseline (ASR_c), $PPI=1 - [ASR_p/ASR_c]$. Because this behavioral test depends on inhibition of the ASR by the test stimulus, and because the strength of the ASR can diminish with age and by advanced hearing loss, it was necessary to exclude mice which did not have statistically significant ASR: a total of 3 CBA mice were excluded, 2 (of 29) at 19 months and 1 (of 8) at 24 months of age; a total of 28 C57 mice were excluded, 4 (of 33) at 4 months, 3 (of 30) at 7 months, 2 (of 37) at 10 months, and 19 (of 24) at 19 months of age. The data of interest were the near-peak mean levels of PPI for each mouse at the longer interstimulus intervals, for the light flash at 70, 110 and 160 ms before the startle, and for the gap in noise at intervals of 60, 110, and 160 ms before the startle.

Auditory Thresholds for Tone Pips: The Auditory Brainstem Response (ABR)

Mice were anaesthetized with ketamine/xylazine (120 mg/kg and 10 mg/kg) then placed on a 10-cm high platform inside a small (57L × 41W × 36H cm), electrically shielded, soundproofed booth (IAC) lined with 4.5 cm-thick echo-attenuating acoustic foam (Sonex®; Illbruck Acoustic). The mouse was arranged in a prone position facing a broad-band electrostatic loudspeaker system (TDT ES1 with ED1 speaker driver) located 10 cm from the head, and was kept warm during the procedure with a circulating-water heating pad. Miniature subdermal needle electrodes (Nicolet) were inserted at the vertex (reference electrode), over the bulla (active electrode), and just above the hind limb (ground electrode). Calibrated tone bursts (5 ms duration, 0.5 ms rise-fall time, phase alternating 90°) were synthesized with SigGenRP© software on a TDT RP2.1 real-time processor, and presented at a rate of 10/s at frequencies of 3, 6, 12, 24, 32, and 48 kHz. The software included an artifact detector that rejected outlier responses. Average ABR waveforms (150 repetitions × 2 duplicates) were recorded at each tested frequency/amplitude combination and filtered from 3 Hz to 1000 Hz. Each 10 ms waveform was comprised of 500 points (0.02 ms sample period). At each frequency, the amplitude of the signal was automatically attenuated (TDT PA5) in 5 dB steps between samples from 90 dB SPL (but 80 dB SPL maximum at 48 kHz) until the wave IV–V complex of the ABR waveform was no longer visually distinguishable from background in duplicate traces in the judgment of a highly experienced technician. By convention, threshold was established as the response at 5 dB above this final level.

Immunocytochemical Electron Microscopy (EM)

During the daytime portion of the light/dark cycle, cohorts of 3-month and 20-month old C57 and CBA mice (n=3 littermate mice from each age and strain) were deeply anesthetized with sodium pentobarbital (80 mg/kg, i.p.) and perfused through the aortic arch with 3.5% acrolein (in 100 mM phosphate buffer (PB), pH 7.4) followed by 4% paraformaldehyde (PFA; in 100 mM PB, pH 7.4). Transverse sections of the brain (50 μm thick) were cut with a vibratome in ice-cooled phosphate-buffered saline (PBS; 0.9% NaCl in 50 mM phosphate buffer, pH 7.4) and immunostained with a rabbit anti-ionized calcium binding adaptor molecule 1 (IBA1) antibody (1:1000 in blocking solution; Wako Pure Chemical Industries) as previously described (Tremblay et al. 2010a; Tremblay et al. 2010b). Briefly, labeling was revealed with 3,3′-diaminobenzidine (DAB; 0.05 mg/ml) and hydrogen peroxide (0.03% in buffer solution; DAB Peroxidase Substrate Kit; Vector Laboratories). Immunostained sections were post-fixed flat in 1% osmium tetroxide, dehydrated in ascending concentrations of ethanol, impregnated in Durcupan (Electron Microscopy Sciences) overnight at RT, mounted between ACLAR embedding films (Electron

Microscopy Sciences), and cured at 55 °C for 48 h. Areas of V1 and A1, at a level approximating the transverse planes A +0.16 to A +0.72 (Franklin and Paxinos 2008), were excised from the same embedded sections, reembedded at the tip of resin blocks, cut with an ultramicrotome (Reichert Ultracut E) at 65–80 nm thickness, collected on bare square-mesh grids, and examined with a Hitachi 7650 transmission electron microscope.

In each animal, pictures were randomly taken in layers II/III of both V1 and A1, at 6,000x and 30,000x, for a total surface of >10,000 μm^2 acquired per region/animal. Neurons, microglia, astrocytes, oligodendrocytes and myelinated axons were identified according to criteria previously defined (Peters et al. 1991b; Peters and Sethares 2004). Neurons with multiple features of degenerating cells, such as dark nuclei and cytoplasm, ruffling of the plasma membrane, dilation of the endoplasmic reticulum, and extensive invagination of the nuclear membrane, were referred to as “dark” neurons (Norman et al. 2008; Oster-Granite et al. 1996; Turmaine et al. 2000; Yang et al. 2008). In addition to their immunoreactivity for the microglia-specific marker IBA1 (Ito et al. 1998), microglia were distinguished from oligodendrocytes by their paler cytoplasm, distinctive long stretches of endoplasmic reticulm, frequent vacuoles and cellular inclusions, irregular contours with obtuse angles, and smaller elongated nucleus delineated by a narrow nuclear cistern (Tremblay et al. 2010a). Quantitative analysis was carried out with ImageJ software (National Institutes of Health). Neurons, “dark” neurons, microglia, astrocytes and oligodendrocytes were counted in all the pictures for a total of 818 cells analyzed. In each of these cells, lysosomal inclusions typically containing electron-dense lipopigments associated with vacuoles (Peters et al. 1991b) were counted. In microglia, large vesicles, vacuoles, lipid droplets, and profiles of cellular elements (Tremblay et al. 2010a) were also counted.

Immunocytochemical Light Microscopy (LM)

For immunocytochemistry and histochemistry, cohorts of 5 CBA mice (n = 15) from three age groups (3–4, 12–13, 20–28 months) and 6 C57 mice (n = 18) from three age groups (3–4, 12–14, 24–28 months) were used. These age groups are referred to as 3 mo, 12 mo and 24 mo old mice in the figures. As previously described (Zettel et al. 2007), mice were taken during the daytime portion of the light/dark cycle and deeply anesthetized with sodium pentobarbital (80 mg/kg, i.p.) and perfused for 25 min with 4% PFA. The brains were removed, postfixed in 4% PFA overnight, and cryoprotected using successive solutions of 10 and 30% sucrose in PBS. Forty-micrometer-thick frozen sections were cut and stored in cryoprotectant at −20°C until the histological reactions.

Microglia were visualized by incubating free floating sections in rabbit anti-IBA1 antibody (1:1000; Wako Pure Chemical Industries) overnight followed by standard DAB immunocytochemistry using an anti-rabbit peroxidase kit and a DAB peroxidase substrate kit (Vector Laboratories). The reaction product was intensified using nickel sulfate to optimize the visualization of very fine processes. Sections from all mice of each strain were reacted together in sectioned dishes to ensure uniform experimental parameters and the analyses were conducted blind. Four sections were analyzed for each of A1 or V1 regions in each mouse. Gray scale photomicrographs were captured using a Spot Insight Color digital camera (Diagnostic Instruments).

Microglia Cell Counts and Nearest Neighbor Analysis

Images were captured using a 10x objective lens (Olympus UPlanFL, 0.3 NA) and processed with ImageJ to determine cellular densities (number of cells/mm^2) and provide cellular coordinates for the analysis of nearest neighbor using custom algorithms in Matlab (Mathworks). Across all cortical layers of A1 or V1 (Franklin and Paxinos 2008), the center of each microglia was marked with a dot using the ImageJ automark function, which

automatically recorded cell numbers as well as spatial coordinates. Location coordinates were entered into Matlab where the distance between each microglia and its nearest neighbor was determined and averaged for all microglia in the image. A spacing index was calculated as the square of the average nearest neighbor distance multiplied by microglial density on a per image basis. This value was then averaged across all images to determine the value per animal.

Morphological Analysis of Individual Microglia Soma

For the morphological analysis of individual microglia, images were captured using a 20x objective lens (Olympus, UPlanFL 0.5 NA) and a total of 30 microglia were analyzed for each area in each mouse of the study. To keep imaging across subjects uniform we focused our analysis in layers II/III and only choose cells that were perfectly in focus. Every IBA1-immunopositive microglia in a particular photomicrograph was analyzed before moving on to the next image as to not introduce selection bias. The soma area was determined by drawing a line around the cell body using the ImageJ freeform tool and allowing the program to automatically calculate the area. Arbor area was determined by using the trapezoid tool to manually connect the most distal points of the processes of each microglia. Arbor circularity was calculated using the formula: (arbor length − width)/(length + width). Therefore the closer the circularity value was to zero, the rounder the arbor. Furthermore, a morphological index (MI) was determined using the formula: soma area/arborization area. The larger the value, the greater the soma size was in relation to the arbor size.

TUNEL and Fluoro-Jade B Histochemistry

Alternate sections from the light immunocytochemistry portion of this experiment were used to examine neuronal necrosis and apoptosis. Sections containing both A1 and V1 from every mouse in the study were mounted on a slide containing at least one section from each age and strain (minimum of six sections/slide) to provide an appropriate internal control. Each slide included as a positive control a brain section from a mouse that received an intrahippocampal lipopolysaccharide injection (LPS; 100 μg) 2 days before perfusion. Apoptotic neurons were visualized using a TUNEL kit (Millipore, Billerica, MA) following the included standardized protocol. Briefly the sections were post fixed for 5 min with a mixture of 95% ethanol and 5% glacial acetic acid, quenched for 5 min with 3% hydrogen peroxide, incubated for 1 h in terminal deoxynucleotidyl transferase enzyme, and incubated in anti-digoxigenin peroxidase in a humidified chamber for 30 min. Sections were then reacted using a standard DAB peroxidase substrate kit (Vector Laboratories) and counterstained with Methyl Green. The positive control had numerous purple apoptotic cells against a green background, but no experimental mice showed TUNEL-positive neurons. No further analysis was performed. To test for necrosis, the sections were stained with Fluoro-Jade B (Millipore), which labels apoptotic and necrotic neurons, using the included standardized protocol. Briefly, sections were incubated in 0.06% Potassium Permanganate for 15 min and incubated in the dark with 0.001% Fluoro-Jade B for 30 min. Numerous necrotic neurons from the LPS-injected control section appeared as green fluorescent cells around the injury site. No necrotic neurons were found in experimental subjects.

Statistical analysis

EM and LM analyses were performed with Prism 5 software (GraphPad). For all statistical tests, sample size (n) represents individual animals. Significance was set to $p<0.05$ and determined using two-way ANOVA with a Bonferroni *post hoc* test to compare across ages and regions. ASR and ABR data were analyzed using an ANOVA provided in the SPSS software (v18, IBM, Somers NY). For ASR analysis, the significance of the observed differences in mean PPI between groups and conditions was assessed by a mixed-design ANOVA in which Lead Time (LT) of the prepulse was a within-subject variable while Age

(A) and Strain (S) were between-subject variables. The degrees of freedom for the repeated measures ANOVA were adjusted for non-homogeneity of between-cell correlations by the Hunyh-Feldt procedure.

Results

Assessment of Auditory and Visual Function in C57 and CBA Mice

We first assayed visual and auditory perception in the two strains of mice at different ages from early adulthood into senescence (Figure 1; also see Supporting information for more details). Behavioral testing used the phenomenon of "reflex modification" to assess age-related changes in sensitivity to auditory or to visual stimuli, by measuring changes in the extent by which these stimuli inhibited the expression of an acoustic startle reflex that was elicited at brief intervals after their presentation (Ison 2001). While this acoustic behavioral test has been used often for assessing auditory processing in mice, the light flash has been previously used in rats to demonstrate the developmental course of loss of vision in young adult RCS rats homozygous for the *rd* gene (Wecker and Ison 1986), and the slower processing of photic stimuli in aging rats (Ison et al. 1991).

These behavioral assays revealed a minimal difference in photic sensitivity between the two strains during young adulthood, in agreement with previous observations (Caruso et al. 2010; Danciger et al. 2007; Williams and Jacobs 2007), but the two groups separated as performance increased with advancing age in the C57 mice and steadily decreased in the CBA mice between 4 and 19 months of age (Figure 1A). In contrast, the CBA mice displayed a greater sensitivity to the acoustic stimulus that was present even in the youngest mice, and the difference between the groups increased with advancing age as performance was maintained in the CBA mice but decreased between 4 and 10 months of age in the C57 mice (Figure 1B). Additionally, auditory function as assayed using ABRs showed no significant difference between the strains at 2 months of age, but differences emerged within the first year of life, as thresholds for the C57 mice rapidly increased, especially at high frequency, but were stable for the CBA mice. By the end of the second year the thresholds for the C57 mice were beyond the intensity limits of our instruments (> 90 dB SPL) while the thresholds for the CBA mouse were minimally affected by just 10 to 15 dB (Figure 1C). Together, these results reveal that the C57 mice display reduced auditory function but relatively well maintained visual function during normal aging, while the CBA mice undergo a converse age-related deficit in vision but well maintained audition.

Cellular and Subcellular Changes in Neurons

To determine how these changes in sensory perception influence neuronal function in corresponding sensory cortices, we examined layers II/III of V1 and A1, where changes in neuronal and glial function have been previously described in younger animals during sensory deprivation (Hensch 2005; Tremblay et al. 2010a) Quantitative analysis in the same C57 and CBA mice at 3 and 20 months of age revealed a slight but not statistically significant decrease in neuronal density during aging in both regions and strains (Table 1) in agreement with previous stereological observations in aged neocortex and hippocampus of several species including humans (reviewed in Morrison and Hof 1997). Nevertheless, neuronal cell bodies often presented signs of senescence in the form of lysosomal inclusions (Figure 2A,B; also see Riga et al. 2006) which became more prevalent during aging, in V1 (Figure 2E, Table 1) and A1 (Figure 2E, Table 1) in both strains. Accumulations of ultrastructurally intact mitochondria within neuronal cell bodies, which could indicate oxidative stress or an early stage of neuronal degeneration (Al-Abdulla and Martin 1998), were also observed (Figure 2B). Additionally, cells with a condensed, electron-dense cytoplasm and nucleoplasm displaying multiple features of degenerating neurons described

in neurodegenerative disease (Oster-Granite et al. 1996; Turmaine et al. 2000; Yang et al. 2008) were sometimes encountered (see Materials and Methods; Figure 2E,F), especially in A1 of the aged and very deaf C57 mice (Figure 2F–G, Table 1). Consistent with previous observations these dark neurons were not undergoing apoptosis nor necrosis, as shown by the absence of TUNEL and Fluoro-Jade B staining on sections from both young (3 and 12 month) and aged (24 month) sensory cortices of either strain (Supporting Figure 1). Together, these observations suggest a particular form of neuronal stress or degeneration that could be specific to the age-related loss of sensory function.

Cellular and Subcellular Changes in Microglia

IBA1-labeled microglia exhibited distinct changes in density, distribution and morphology during aging, depending on the strain and cortical area. In C57 mice, microglia became more numerous throughout cortical layers I to VI in both V1 and A1 at 24 months of age (Figure 3G; Table 2). This increase in microglial density was more pronounced in A1 than in V1 suggesting that loss of auditory input could exacerbate microglial proliferation during aging (Peters et al. 1991a; Vaughan and Peters 1974). We also found an age-related decrease in the distance between neighboring microglia in both A1 and V1 (reduced spacing index; Figure 3A–F,H; Table 2), which could not be accounted for by their increased density, thus suggesting that microglia are less evenly distributed in aged cortices irrespective of sensory input. In contrast with previous observations in young adult mice (Lawson et al. 1990), microglial cell bodies in aged mice often localized close together and sometimes in direct contiguity (see Figure 3C and F for examples) which could be suggestive of ongoing proliferation. In CBA mice, a progressive age-related decrease in microglial nearest neighbor distance was also observed at 12 and 24 months of age to similar degrees in A1 and V1 (reduced spacing index) whereas microglial density remained relatively constant (Figure 3I–P; Table 2), indicating a loss of territorial organization that could be regulated independently from microglial density during aging or age-related sensory loss.

Microglia showed remarkable morphological transformation over the course of aging in cortical layers II/III (Figures 4–5). In C57 mice, at 24 months of age, microglial process arborizations were significantly reduced in area, and displayed elongated geometries as evidenced by an increased circularity index (Figure 4A–H, Table 2). A morphological index was computed to assess the soma area relative to the process area (soma area/arborization area), two parameters susceptible to change during microglial activation (Streit et al. 1999). Aged microglia displayed significantly increased morphological indices that were most pronounced in A1 (Figure 4I; Table 2), suggesting an association with hearing loss. Since microglial soma area displayed little variation during aging or age-related sensory deficit (Figure 4J; Table 2), these changes in morphological index most likely resulted from the reduction in the area of microglial arborizations. Nevertheless, microglial somas in the oldest animals were more variable in size: comparisons of their standard deviation showed a significant increase at 24 months of age especially in A1 (Figure 4K; Table 2). This effect in turn translated into significant differences in the standard deviation of the morphological index with age (Figure 4L; Table 2). In the CBA mice, microglia also underwent striking morphological changes as early as 12 months (Figure 5; Table 2), with a more complex profile. The span of microglial process arborizations decreased with age and became more elongated (Figure 5A–H; Table 2) as in C57 animals, and there was a trend towards smaller microglial arborizations at all ages in V1. Morphological indices were also significantly increased during aging, especially at 24 months of age (Figure 5I; Table 2), suggesting that microglial morphology could also be modulated in an age and activity-dependent manner in this strain. These changes in morphological indices occurred in the absence of changes in microglial soma areas except for an increase in standard deviations at 24 months of age as in the C57 mice (Figure 5J–L; Table 2). Together, these observations in both mouse strains

suggest that microglia are differentially sensitive to aging and age-related sensory loss, with different populations undergoing diverse structural and functional changes in parallel.

Ultrastructural examination also revealed distinctive features that were most pronounced in layers II/III in V1 of CBA mice and A1 of C57 mice at 20 months of age such as hypertrophy and rounding of the cell body (Figure 6B,C and 7A,C), enlargement of processes (Figure 7E,F) and accumulation of various types of phagocytic inclusions (Figure 6A,C,D and Figure 7). While microglial processes were often found in direct juxtaposition with synapse-associated dendritic spines, axon terminals, synaptic clefts and perisynaptic astrocytic processes throughout adulthood and aging (see Supporting Figure 2), as previously shown in adolescent and young adult mice (Tremblay et al. 2010a; Wake et al. 2009), microglial cell bodies and large processes often contained cellular inclusions that resembled profiles of axon terminals (Figure 7A–F) or dendritic spines (Figure 7E) sometimes separated by wide electron-lucent space (Figure 7E). Microglial processes extending between axon terminals and dendrites (Figure 7F) in a way reminiscent of synaptic stripping during acute and inflammatory lesions (Trapp et al. 2007) were also observed. Furthermore, quantitative analysis of the total number of inclusions (lysosomal lipopigments, large vesicles, vacuoles, lipid droplets, and cellular elements sometimes displaying ultrastructural features of axon terminals and dendritic spines) revealed an increased prevalence during aging, in V1 of the CBA mice and A1 of the C57 mice (Figure 6E, Table 1), with nearly all microglia containing inclusions. Some microglia appeared almost completely filled with cellular debris, akin to fat granule cells or *gitter* cells (9 out of 45 microglia; see Figure 6C for an example; Vaughan and Peters 1974), indicating that microglial phagocytosis of cellular elements including synapses could become accelerated during age-related loss of sight or hearing.

Changes in other Glial Components: Astrocytes, Oligodendrocytes, and Axonal Myelination

In contrast with microglia, astrocytes showed little change in number or morphology during aging or age-related sensory loss (Figure 8A,B; Table 1), in layers II/III of V1 and A1, in agreement with previous observations in aged rat cerebral cortex (Vaughan and Peters 1974). While some astrocytic processes ensheathing synapses and blood vessels appeared enlarged during aging (Figure 8A), similar to reactive astrocytes which become hypertrophic (Wilhelmsson et al. 2006), the most apparent change was the occasional accumulation of large lysosomal inclusions associated with vacuoles (see Figure 8B for example in an astrocytic process) in A1 of the very deaf C57 mice (Table 1). In contrast, oligodendrocytes rarely contained lysosomal inclusions (Figure 8C,D) but increased in number and were more often encountered in contiguous pairs during aging, particularly in V1 of the CBA mice (Table 1), as previously reported in aged rhesus monkeys (Peters and Sethares 2004), suggesting an ongoing proliferation that could be exacerbated by age-related sensory loss in both strains. Lastly, our ultrastructural analysis also revealed alterations of myelinated axons during aging, also in V1 of the CBA mice and A1 of the C57 mice especially. Some myelin sheaths appeared ballooned (Figure 8F) as during natural and experimental demyelination (Peters and Sethares 2003), while other axons displayed redundant myelin sheaths (Figure 8E,F) suggesting oligodendrocytic attempts at remyelination in the context of cortical senescence (Peters and Sethares 2004).

Discussion

Different mouse strains experience age-related hearing and/or sight loss to different degrees. While C57 and CBA mice are known to differentially develop hearing deficits during normal aging, here we also report reciprocal differences in their visual sensitivity with a behavioral assay that depends on the inhibition of the acoustic startle reflex by innocuous

and even near threshold prestimulation (Hoffman and Ison 1992). Whether and how these changes in sensory perception impact neuronal and glial function in corresponding sensory cortices is the focus of this discussion. It is important to note that while functional changes in sensory perception were detected within the first year of age, the cellular changes in A1 of the C57 and V1 of the CBA mice were first observed at 20 and 12 months of age respectively, suggesting that loss of peripheral function precedes and likely drives central changes. Nevertheless, we cannot rule out that microglial changes in the cortex or lower structures also contribute to loss of sensory function.

Effects of Aging on Cortical Cells

Aging is a risk factor for most neurological disorders (Merrill and Small 2011), and various cellular and subcellular changes that occur within the aging brain can alter function in the absence of pathology. Possible sources of these changes include accumulated DNA damage (Gaubatz 1995; Vijg and Campisi 2008), oxidative stress (Droge and Schipper 2007), deregulated calcium homeostasis and signaling (Disterhoft et al. 1994; O'Neill et al. 1997; Zettel et al. 1997), as well as altered neuroimmune function (von Bernhardi et al. 2010). The idea that brain dysfunction during aging is mediated by a large-scale loss of central neurons has now been largely discredited although a more subtle region-specific loss may occur (West 1993; Willott et al. 1994; Woodruff-Pak et al. 2010). Similarly, biophysical properties of neurons appear to be largely conserved across the lifespan (Barnes and McNaughton 1980; Burke and Barnes 2006) aside from an increase in calcium conductance that could contribute to altered plasticity mechanisms (Barnes et al. 2000; Landfield et al. 1978) and increased susceptibility to dendritic remodeling and synaptic elimination (Barnes et al. 1992; Geinisman et al. 1992). In this context, our ultrastructural analysis showed relatively unchanged neuronal numbers during aging in A1 and V1 of both mouse strains that were nevertheless accompanied by various signs of neuronal stress. These included the prevalence of lysosomal inclusions, which were previously associated with protease instability, lysosome and cellular recycling dysfunction, cytoskeletal damage, amyloid deposits and amyloid-related neuropathology (Riga et al. 2006; Brunk and Terman 2002), and the accumulation of morphologically intact mitochondria within neuronal cell bodies (Al-Abdulla and Martin 1998). Together, our observations thus suggest that aged neurons may have altered metabolic function without undergoing large scale degeneration.

The most profound age-related change that we observed concerned microglia, the resident immune cells of the brain, which are the key mediators of neuroinflammatory processes within the CNS in various contexts including aging (Lee et al. 2000; Prinz et al. 2011; Streit 2002; von Bernhardi et al. 2010). In particular, we found that microglia become more numerous and tend to distribute less evenly, with an increased prevalence of direct contiguities, suggesting an increased proliferation of microglia and/or a breakdown of the mechanisms which maintain microglial territories and regulate immune surveillance (Nimmerjahn et al. 2005). Aged microglia also exhibited morphological changes that were similar to those previously described during pathological activation (Streit et al. 1999): a general simplification of the microglial arbor with a decrease in the span of microglial processes compared to the cell body. Our findings are supported by recent live confocal imaging observations showing that aged microglia in retinal explants have increased density, decreased arbor area, together with decreased total number of branch points and total process length (Damani et al. 2011). Such morphological changes may reflect age-induced microglial activation as suggested by the increased expression of molecular markers of activation in the aged brain (Ogura et al. 1994; Sheffield and Berman 1998; Sierra et al. 2007), although dystrophic changes differing morphologically from microglial activation were also reported during aging (Streit et al. 2004). Future quantitative morphological analyses, such as those described here, could contribute to defining the exact morphological

parameters that characterize different modes of microglial function, including activation and dystrophy, and further refine our understanding of the nature of microglial transformation during aging (Sierra et al. 2007). While microglial cell body size was not significantly altered, we observed greater variation in the size of microglial somas in older animals, suggesting that populations of aged microglia may become more heterogeneous and that distinct types of morphological and behavioral changes may occur in parallel. This is all the more intriguing in the context of the recent interest in defining subpopulations of microglia (Carson et al. 2007; Lynch 2009) implementing different molecular signaling cascades on different timescales, with pro- and anti-inflammatory functions that can exacerbate or ameliorate neuronal injury (Kigerl et al. 2009). While the expression of both pro- and anti-inflammatory cytokines increases with aging (Sierra et al. 2007), it is currently unknown whether such heterogeneous microglial populations exist in the aged brain and how they could impact age-related functional decline. In future experiments, it will be important to tie morphological alterations with an assessment of microglial expression of cytokines, chemokines and other functional markers *in situ*, to provide further insights into the beneficial and/or detrimental effects of microglia on age-related functional decline.

Effect of Sensory Deprivation on Aged Cortical Cells

Activity-dependent plasticity in sensory subcortical and cortical areas has been extensively studied in young animals (Rittenhouse and Majewska 2009), but the impact of age-related sensory loss on the aging process is still not clear. The secretion of neuroprotective agents such as growth factors is activity-dependent (Caleo and Maffei 2002), and changes in neuronal activity induce homeostatic changes that could affect the aging process (Desai et al. 1999; Turrigiano and Nelson 2004). In fact, many of the molecular changes observed in aged neuronal networks can be replicated by silencing cortical neurons (Gleichmann et al. 2010), suggesting that sensory deprivation could affect neuronal function and exacerbate age-related changes in a similar manner.

A surprising finding in our study was the increased prevalence of “dark” neurons in deprived A1 of the C57 mice undergoing age-related loss of hearing. These apparently degenerating cells were neither necrotic nor apoptotic and contained large numbers of lysosomal inclusions suggesting metabolic dysfunction (Riga et al. 2006). Similar dark neurons have been described in Alzheimer’s and Huntington’s diseases (Oster-Granite et al. 1996; Turmaine et al. 2000; Yang et al. 2008) and after chronic inhibition of long-term potentiation/cAMP-response element-binding protein (CREB) function (Valor et al. 2010). Interestingly CREB is downregulated in various neurodegenerative diseases including Alzheimer’s and Huntington’s, as well as during normal aging (Bach et al. 1999; Porte et al. 2008; Shimohata et al. 2000; Tomobe et al. 2007; Vitolo et al. 2002). Since this cellular “darkening” can be reversible in certain conditions (Auer et al. 1985; Ingvar et al. 1988), it presently remains unclear whether the “dark” neurons that we observed were undergoing cellular stress or degeneration in the aging brain.

Our results also showed consistent effects of age-related sensory loss on microglia in both C57 and CBA mice. Recent findings have shown that neuroimmune molecular pathways contribute to synaptic plasticity (Boulanger and Shatz 2004), and changes in microglial morphology and behavior have been described during visual deprivation in adolescent and adult mice (Tremblay et al. 2010a; Wake et al. 2009) suggesting they are a general consequence of sensory loss. While lysosomal inclusions were observed in all types of cells except oligodendrocytes, and appear to be a normal consequence of aging (Riga et al. 2006), aged microglia accumulated exceptionally large amounts of lysosomal inclusions, including profiles resembling synaptic elements, in cortical areas deprived of sensory input. This striking behavior suggests an accumulated phagocytic activity, supporting previous observations that microglia enlarge and become filled with cellular debris during normal

aging (Peters 2002), a phenomenon which could eventually contribute to an impairment of their phagocytic clearance (Neumann et al. 2009). Complete loss of vision during adolescence also resulted in increased microglial phagocytosis of synaptic elements, and in an overall decrease in microglial motility in visual cortex (Tremblay et al. 2010a), and similarly, a reduced velocity of individual microglial processes was recently observed with live confocal imaging in retinal explants from aged mice (Damani et al. 2011). Microglia were also shown to contribute to synaptic pruning during early postnatal development (Paolicelli et al. 2011). Together these findings support a model in which quiescent microglia contribute to restructuring neuronal circuits by eliminating synapses in an experience-dependent manner throughout the lifespan. Future experiments involving two-photon *in vivo* imaging of microglia could further explore their novel physiological role in aging.

Lastly, our analysis also revealed ultrastructural evidence of demyeination and remyelination in deprived sensory cortices of the C57 and CBA mice, suggesting that axonal dysfunction and/or myelin remodeling could be exacerbated by the loss of sensory function during normal aging. We also found increased numbers of oligodendrocytes that were often contiguous one with another, possibly suggesting their proliferation, as previously reported in aged rhesus monkeys (Peters and Sethares 2004). In line with these observations, myelin remodeling was recently shown to be regulated by neuronal activity and sensory-experience dependent plasticity (Fields 2010; McGee et al. 2005; Wake et al. 2011). Since newborn oligodendrocytes are derived in the mature brain from oligodendrocytic progenitors sharing few ultrastructural features with oligodendrocytes (Peters and Sethares 2004) but specifically expressing the NG2 chondroitin sulfate proteoglycan (Trotter et al. 2010), it will be important in subsequent experiments to examine these oligodendrocytic progenitors and their differential changes in terms of morphology and behavior during aging and age-related sensory loss.

Supplementary Material

Refer to Web version on PubMed Central for supplementary material.

Acknowledgments

This work was supported by grants from the NIH EY019277, Whitehall Foundation, the Alfred P. Sloan Foundation, and a Career Award in the Biomedical Sciences from the Burroughs Wellcome Fund to AKM, by NIH-NIA research grant (AG09534), NIH center grants from the NIDCD (P30 DC05409) and the NEI (P30 EY01319), and the Schmitt Program for Integrative Brain Research. MET was funded by Fonds de la Recherche en Santé du Quebéc (FRSQ) and Canadian Institutes of Health Research (CIHR) postdoctoral fellowships. We are grateful to John A. Olschowka and his laboratory for providing LPS-injected brain samples, Robert D. Frisina for mice, and Kathy Barsz for statistical advice.

References

Al-Abdulla NA, Martin LJ. Apoptosis of retrogradely degenerating neurons occurs in association with the accumulation of perikaryal mitochondria and oxidative damage to the nucleus. Am J Pathol. 1998; 153:447–56. [PubMed: 9708805]

Anderson JM, Hubbard BM, Coghill GR, Slidders W. The effect of advanced old age on the neurone content of the cerebral cortex. Observations with an automatic image analyser point counting method. J Neurol Sci. 1983; 58:235–46. [PubMed: 6834079]

Auer RN, Kalimo H, Olsson Y, Siesjo BK. The temporal evolution of hypoglycemic brain damage. I. Light- and electron-microscopic findings in the rat cerebral cortex. Acta Neuropathol. 1985; 67:13–24. [PubMed: 4024866]

Bach ME, Barad M, Son H, Zhuo M, Lu YF, Shih R, Mansuy I, Hawkins RD, Kandel ER. Age-related defects in spatial memory are correlated with defects in the late phase of hippocampal long-term

potentiation in vitro and are attenuated by drugs that enhance the cAMP signaling pathway. Proc Natl Acad Sci U S A. 1999; 96:5280–5. [PubMed: 10220457]

Barnes CA, McNaughton BL. Physiological compensation for loss of afferent synapses in rat hippocampal granule cells during senescence. J Physiol. 1980; 309:473–85. [PubMed: 7252877]

Barnes CA, Rao G, Foster TC, McNaughton BL. Region-specific age effects on AMPA sensitivity: electrophysiological evidence for loss of synaptic contacts in hippocampal field CA1. Hippocampus. 1992; 2:457–68. [PubMed: 1284976]

Barnes CA, Rao G, Houston FP. LTP induction threshold change in old rats at the perforant path-granule cell synapse. Neurobiol Aging. 2000; 21:613–20. [PubMed: 11016529]

Bilbo SD. Early-life infection is a vulnerability factor for aging-related glial alterations and cognitive decline. Neurobiol Learn Mem. 2010; 94:57–64. [PubMed: 20388544]

Boulanger LM, Shatz CJ. Immune signalling in neural development, synaptic plasticity and disease. Nat Rev Neurosci. 2004; 5:521–531. [PubMed: 15208694]

Brunk UT, Terman A. The mitochondrial-lysosomal axis theory of aging: accumulation of damaged mitochondria as a result of imperfect autophagocytosis. Eur J Biochem. 2002; 269:1996–2002. [PubMed: 11985575]

Burke SN, Barnes CA. Neural plasticity in the ageing brain. Nat Rev Neurosci. 2006; 7:30–40. [PubMed: 16371948]

Caleo M, Maffei L. Neurotrophins and plasticity in the visual cortex. Neuroscientist. 2002; 8:52–61. [PubMed: 11843099]

Carson MJ, Bilousova TV, Puntambekar SS, Melchior B, Doose JM, Ethell IM. A rose by any other name? The potential consequences of microglial heterogeneity during CNS health and disease. Neurotherapeutics. 2007; 4:571–9. [PubMed: 17920538]

Caruso RC, Aleman TS, Cideciyan AV, Roman AJ, Sumaroka A, Mullins CL, Boye SL, Hauswirth WW, Jacobson SG. Retinal disease in Rpe65-deficient mice: comparison to human leber congenital amaurosis due to RPE65 mutations. Invest Ophthalmol Vis Sci. 2010; 51:5304–13. [PubMed: 20484585]

Clapcote SJ, Lazar NL, Bechard AR, Roder JC. Effects of the rd1 mutation and host strain on hippocampal learning in mice. Behav Genet. 2005; 35:591–601. [PubMed: 16184487]

Congdon N, O'Colmain B, Klaver CC, Klein R, Munoz B, Friedman DS, Kempen J, Taylor HR, Mitchell P. Causes and prevalence of visual impairment among adults in the United States. Arch Ophthalmol. 2004; 122:477–85. [PubMed: 15078664]

Cragg BG. The density of synapses and neurons in normal, mentally defective ageing human brains. Brain. 1975; 98:81–90. [PubMed: 123474]

Dalke C, Loster J, Fuchs H, Gailus-Durner V, Soewarto D, Favor J, Neuhauser-Klaus A, Pretsch W, Gekeler F, Shinoda K, et al. Electroretinography as a screening method for mutations causing retinal dysfunction in mice. Invest Ophthalmol Vis Sci. 2004; 45:601–9. [PubMed: 14744904]

Damani MR, Zhao L, Fontainhas AM, Amaral J, Fariss RN, Wong WT. Age-related alterations in the dynamic behavior of microglia. Aging Cell. 2011; 10:263–76. [PubMed: 21108733]

Danciger M, Yang H, Ralston R, Liu Y, Matthes MT, Peirce J, Lavail MM. Quantitative genetics of age-related retinal degeneration: a second F1 intercross between the A/J and C57BL/6 strains. Mol Vis. 2007; 13:79–85. [PubMed: 17277741]

Desai NS, Rutherford LC, Turrigiano GG. BDNF regulates the intrinsic excitability of cortical neurons. Learn Mem. 1999; 6:284–91. [PubMed: 10492010]

Disterhoft, JF.; Gispen, WH.; Traber, J.; Khachaturian, ZF. Calcium hypothesis of aging and dementia. New York: New York Academy of Sciences; 1994.

Droge W, Schipper HM. Oxidative stress and aberrant signaling in aging and cognitive decline. Aging Cell. 2007; 6:361–70. [PubMed: 17517043]

Fields RD. Neuroscience. Change in the brain's white matter. Science. 2010; 330:768–9. [PubMed: 21051624]

Flanary BE, Sammons NW, Nguyen C, Walker D, Streit WJ. Evidence that aging and amyloid promote microglial cell senescence. Rejuvenation Res. 2007; 10:61–74. [PubMed: 17378753]

Franklin, KBJ.; Paxinos, G. The Mouse Brain in Stereotaxic Coordinates. Academic Press; 2008.

Gaubatz, JW. Genomic instability during aging of postmitotic mammalian cells. In: Macieira-Coelho, A., editor. Molecular Basis of Aging. Boca Raton: CRC Press; 1995. p. 71-182.

Geinisman Y, deToledo-Morrell L, Morrell F, Persina IS, Rossi M. Age-related loss of axospinous synapses formed by two afferent systems in the rat dentate gyrus as revealed by the unbiased stereological dissector technique. Hippocampus. 1992; 2:437–44. [PubMed: 1308200]

Gleichmann M, Zhang Y, Wood WH 3rd, Becker KG, Mughal MR, Pazin MJ, van Praag H, Kobilo T, Zonderman AB, Troncoso JC, et al. Molecular changes in brain aging and Alzheimer's disease are mirrored in experimentally silenced cortical neuron networks. Neurobiol Aging. 2010

Henry KR, Chole RA. Genotypic differences in behavioral, physiological and anatomical expressions of age-related hearing loss in the laboratory mouse. Audiology. 1980; 19:369–83. [PubMed: 7436856]

Hensch TK. Critical period plasticity in local cortical circuits. Nat Rev Neurosci. 2005; 6:877–88. [PubMed: 16261181]

Hof PR, Morrison JH. The aging brain: morphomolecular senescence of cortical circuits. Trends Neurosci. 2004; 27:607–13. [PubMed: 15374672]

Hoffman, HS.; Ison, JR. Reflex modification and the anlaysis of sensory processing in developmental and comparative research. In: Campbell, BA.; Hayne, H.; Richardson, R., editors. Attention and information processing in infants and adults: perspectives from human and animal research. Hillsdale: Lawrence Erlbaum Associates; 1992.

Hunter KP, Willott JF. Aging and the auditory brainstem response in mice with severe or minimal presbycusis. Hear Res. 1987; 30:207–18. [PubMed: 3680066]

Inamizu T, Chang MP, Makinodan T. Influence of age on the production and regulation of interleukin-1 in mice. Immunology. 1985; 55:447–55. [PubMed: 3874817]

Ingvar M, Morgan PF, Auer RN. The nature and timing of excitotoxic neuronal necrosis in the cerebral cortex, hippocampus and thalamus due to flurothyl-induced status epilepticus. Acta Neuropathol. 1988; 75:362–9. [PubMed: 3364160]

Ison, JR. The acoustic startle response in the mouse: reflex elicitation and reflex modification by preliminary stimuli. In: Willott, JF., editor. Handbook of Mouse Auditory Research: From Behavior to Molecular Biology. Boca Raton: CRC Press; 2001. p. 59-82.

Ison JR, Bowen GP, O'Connor K. Reflex modification produced by visual stimuli in the rat following functional decortication. Psychobiology. 1991; 19:122–126.

Ito D, Imai Y, Ohsawa K, Nakajima K, Fukuuchi Y, Kohsaka S. Microglia-specific localisation of a novel calcium binding protein, Iba1. Brain Res Mol Brain Res. 1998; 57:1–9. [PubMed: 9630473]

Kigerl KA, Gensel JC, Ankeny DP, Alexander JK, Donnelly DJ, Popovich PG. Identification of two distinct macrophage subsets with divergent effects causing either neurotoxicity or regeneration in the injured mouse spinal cord. J Neurosci. 2009; 29:13435–44. [PubMed: 19864556]

Landfield PW, McGaugh JL, Lynch G. Impaired synaptic potentiation processes in the hippocampus of aged, memory-deficient rats. Brain Res. 1978; 150:85–101. [PubMed: 208716]

Lawson LJ, Perry VH, Dri P, Gordon S. Heterogeneity in the distribution and morphology of microglia in the normal adult mouse brain. Neuroscience. 1990; 39:151–70. [PubMed: 2089275]

Lee CK, Weindruch R, Prolla TA. Gene-expression profile of the ageing brain in mice. Nat Genet. 2000; 25:294–7. [PubMed: 10888876]

Li HS, Borg E. Age-related loss of auditory sensitivity in two mouse genotypes. Acta Otolaryngol. 1991; 111:827–34. [PubMed: 1759567]

Luo XG, Ding JQ, Chen SD. Microglia in the aging brain: relevance to neurodegeneration. Mol Neurodegener. 2010; 5:12. [PubMed: 20334662]

Lynch MA. The multifaceted profile of activated microglia. Mol Neurobiol. 2009; 40:139–56. [PubMed: 19629762]

Lynch MA. Age-related neuroinflammatory changes negatively impact on neuronal function. Front Aging Neurosci. 2010; 1:6. [PubMed: 20552057]

McGee AW, Yang Y, Fischer QS, Daw NW, Strittmatter SM. Experience-driven plasticity of visual cortex limited by myelin and Nogo receptor. Science. 2005; 309:2222–6. [PubMed: 16195464]

Merrill DA, Small GW. Prevention in psychiatry: effects of healthy lifestyle on cognition. Psychiatr Clin North Am. 2011; 34:249–61. [PubMed: 21333851]

Morrison JH, Hof PR. Life and death of neurons in the aging brain. Science. 1997; 278:412–9. [PubMed: 9334292]

Neumann H, Kotter MR, Franklin RJ. Debris clearance by microglia: an essential link between degeneration and regeneration. Brain. 2009; 132:288–95. [PubMed: 18567623]

Nimmerjahn A, Kirchhoff F, Helmchen F. Resting microglial cells are highly dynamic surveillants of brain parenchyma in vivo. Science. 2005; 308:1314–8. [PubMed: 15831717]

Norman JP, Perry SW, Reynolds HM, Kiebala M, De Mesy Bentley KL, Trejo M, Volsky DJ, Maggirwar SB, Dewhurst S, Masliah E, et al. HIV-1 Tat activates neuronal ryanodine receptors with rapid induction of the unfolded protein response and mitochondrial hyperpolarization. PLoS One. 2008; 3:e3731. [PubMed: 19009018]

O'Neill WE, Zettel ML, Whittemore KR, Frisina RD. Calbindin D-28k immunoreactivity in the medial nucleus of the trapezoid body declines with age in C57BL/6, but not CBA/CaJ, mice. Hear Res. 1997; 112:158–66. [PubMed: 9367238]

Ogura K, Ogawa M, Yoshida M. Effects of ageing on microglia in the normal rat brain: immunohistochemical observations. Neuroreport. 1994; 5:1224–6. [PubMed: 7919169]

Oster-Granite ML, McPhie DL, Greenan J, Neve RL. Age-dependent neuronal and synaptic degeneration in mice transgenic for the C terminus of the amyloid precursor protein. J Neurosci. 1996; 16:6732–41. [PubMed: 8824314]

Paolicelli RC, Bolasco G, Pagani F, Maggi L, Scianni M, Panzanelli P, Giustetto M, Ferreira TA, Guiducci E, Dumas L, et al. Synaptic pruning by microglia is necessary for normal brain development. Science. 2011; 333:1456–8. [PubMed: 21778362]

Perry VH, Matyszak MK, Fearn S. Altered antigen expression of microglia in the aged rodent CNS. Glia. 1993; 7:60–7. [PubMed: 8423063]

Peters A. Age-related changes in oligodendrocytes in monkey cerebral cortex. J Comp Neurol. 1996; 371:153–63. [PubMed: 8835724]

Peters A. Structural changes that occur during normal aging of primate cerebral hemispheres. Neurosci Biobehav Rev. 2002; 26:733–41. [PubMed: 12470684]

Peters A, Josephson K, Vincent SL. Effects of aging on the neuroglial cells and pericytes within area 17 of the rhesus monkey cerebral cortex. Anat Rec. 1991a; 229:384–98. [PubMed: 2024779]

Peters, A.; Palay, SL.; Webster, H. The fine structure of the nervous system: the neurons and supporting cells. Philadelphia: W.B. Saunders; 1991b.

Peters A, Sethares C. Is there remyelination during aging of the primate central nervous system? J Comp Neurol. 2003; 460:238–54. [PubMed: 12687688]

Peters A, Sethares C. Oligodendrocytes, their progenitors and other neuroglial cells in the aging primate cerebral cortex. Cereb Cortex. 2004; 14:995–1007. [PubMed: 15115733]

Porte Y, Buhot MC, Mons N. Alteration of CREB phosphorylation and spatial memory deficits in aged 129T2/Sv mice. Neurobiol Aging. 2008; 29:1533–46. [PubMed: 17478013]

Prinz M, Priller J, Sisodia SS, Ransohoff RM. Heterogeneity of CNS myeloid cells and their roles in neurodegeneration. Nat Neurosci. 2011; 13:1227–35. [PubMed: 21952260]

Rapp PR, Gallagher M. Preserved neuron number in the hippocampus of aged rats with spatial learning deficits. Proc Natl Acad Sci U S A. 1996; 93:9926–30. [PubMed: 8790433]

Riga D, Riga S, Halalau F, Schneider F. Brain lipopigment accumulation in normal and pathological aging. Ann N Y Acad Sci. 2006; 1067:158–63. [PubMed: 16803981]

Rittenhouse CD, Majewska AK. Synaptic mechanisms of activity-dependent remodeling in visual cortex. J Exp Neurosci. 2009; 2:23–41.

Sharts-Hopko N. Low vision and blindness among midlife and older adults: a review of the nursing research literature. Holist Nurs Pract. 2009; 23:94–100. [PubMed: 19258851]

Sheffield LG, Berman NE. Microglial expression of MHC class II increases in normal aging of nonhuman primates. Neurobiol Aging. 1998; 19:47–55. [PubMed: 9562503]

Sheng JG, Mrak RE, Griffin WS. Enlarged and phagocytic, but not primed, interleukin-1 alpha-immunoreactive microglia increase with age in normal human brain. Acta Neuropathol. 1998; 95:229–34. [PubMed: 9542587]

Shimohata T, Nakajima T, Yamada M, Uchida C, Onodera O, Naruse S, Kimura T, Koide R, Nozaki K, Sano Y, et al. Expanded polyglutamine stretches interact with TAFII130, interfering with CREB-dependent transcription. Nat Genet. 2000; 26:29–36. [PubMed: 10973244]

Sierra A, Gottfried-Blackmore AC, McEwen BS, Bulloch K. Microglia derived from aging mice exhibit an altered inflammatory profile. Glia. 2007; 55:412–24. [PubMed: 17203473]

Streit WJ. Microglia as neuroprotective, immunocompetent cells of the CNS. Glia. 2002; 40:133–9. [PubMed: 12379901]

Streit WJ, Miller KR, Lopes KO, Njie E. Microglial degeneration in the aging brain--bad news for neurons? Front Biosci. 2008; 13:3423–38. [PubMed: 18508444]

Streit WJ, Sammons NW, Kuhns AJ, Sparks DL. Dystrophic microglia in the aging human brain. Glia. 2004; 45:208–12. [PubMed: 14730714]

Streit WJ, Walter SA, Pennell NA. Reactive microgliosis. Prog Neurobiol. 1999; 57:563–81. [PubMed: 10221782]

Tobias JV, Bilger RC, Brody H, Gates GA, Haskell G, Howard D, Marshall LA, Nerbonne MA, Pickett JA. Speech understanding and aging. Working Group on Speech Understanding and Aging. Committee on Hearing, Bioacoustics, and Biomechanics, Commission on Behavioral and Social Sciences and Education, National Research Council. J Acoust Soc Am. 1988; 83:859–95. [PubMed: 3281988]

Tomobe K, Okuma Y, Nomura Y. Impairment of CREB phosphorylation in the hippocampal CA1 region of the senescence-accelerated mouse (SAM) P8. Brain Res. 2007; 1141:214–7. [PubMed: 17303091]

Trapp BD, Wujek JR, Criste GA, Jalabi W, Yin X, Kidd GJ, Stohlman S, Ransohoff R. Evidence for synaptic stripping by cortical microglia. Glia. 2007; 55:360–8. [PubMed: 17136771]

Tremblay ME, Lowery RL, Majewska AK. Microglial interactions with synapses are modulated by visual experience. PLoS Biol. 2010a; 8:e1000527. [PubMed: 21072242]

Tremblay ME, Riad M, Majewska A. Preparation of mouse brain tissue for immunoelectron microscopy. J Vis Exp. 2010b

Trotter J, Karram K, Nishiyama A. NG2 cells: Properties, progeny and origin. Brain Res Rev. 2010; 63:72–82. [PubMed: 20043946]

Turmaine M, Raza A, Mahal A, Mangiarini L, Bates GP, Davies SW. Nonapoptotic neurodegeneration in a transgenic mouse model of Huntington's disease. Proc Natl Acad Sci U S A. 2000; 97:8093–7. [PubMed: 10869421]

Turrigiano GG, Nelson SB. Homeostatic plasticity in the developing nervous system. Nat Rev Neurosci. 2004; 5:97–107. [PubMed: 14735113]

Uemura E. Age-related changes in the subiculum of Macaca mulatta: dendritic branching pattern. Exp Neurol. 1985; 87:412–27. [PubMed: 3972045]

Valor LM, Jancic D, Lujan R, Barco A. Ultrastructural and transcriptional profiling of neuropathological misregulation of CREB function. Cell Death Differ. 2010; 17:1636–44. [PubMed: 20395962]

Vaughan DW, Peters A. Neuroglial cells in the cerebral cortex of rats from young adulthood to old age: an electron microscope study. J Neurocytol. 1974; 3:405–29. [PubMed: 4373545]

Vijg J, Campisi J. Puzzles, promises and a cure for ageing. Nature. 2008; 454:1065–71. [PubMed: 18756247]

Vitolo OV, Sant'Angelo A, Costanzo V, Battaglia F, Arancio O, Shelanski M. Amyloid beta-peptide inhibition of the PKA/CREB pathway and long-term potentiation: reversibility by drugs that enhance cAMP signaling. Proc Natl Acad Sci U S A. 2002; 99:13217–21. [PubMed: 12244210]

von Bernhardi R, Tichauer JE, Eugenin J. Aging-dependent changes of microglial cells and their relevance for neurodegenerative disorders. J Neurochem. 2010; 112:1099–114. [PubMed: 20002526]

Wake H, Lee PR, Fields RD. Control of local protein synthesis and initial events in myelination by action potentials. Science. 2011; 333:1647–51. [PubMed: 21817014]

Wake H, Moorhouse AJ, Jinno S, Kohsaka S, Nabekura J. Resting microglia directly monitor the functional state of synapses in vivo and determine the fate of ischemic terminals. J Neurosci. 2009; 29:3974–3980. [PubMed: 19339593]

Wecker JR, Ison JR. Visual function measured by reflex modification in rats with inherited retinal dystrophy. Behav Neurosci. 1986; 100:679–84. [PubMed: 3778632]

West MJ. Regionally specific loss of neurons in the aging human hippocampus. Neurobiol Aging. 1993; 14:287–93. [PubMed: 8367010]

Wilhelmsson U, Bushong EA, Price DL, Smarr BL, Phung V, Terada M, Ellisman MH, Pekny M. Redefining the concept of reactive astrocytes as cells that remain within their unique domains upon reaction to injury. Proc Natl Acad Sci U S A. 2006; 103:17513–8. [PubMed: 17090684]

Williams GA, Jacobs GH. Cone-based vision in the aging mouse. Vision Res. 2007; 47:2037–46. [PubMed: 17509638]

Willott JF. Effects of aging, hearing loss, and anatomical location on thresholds of inferior colliculus neurons in C57BL/6 and CBA mice. J Neurophysiol. 1986; 56:391–408. [PubMed: 3760927]

Willott JF, Bross LS, McFadden SL. Morphology of the inferior colliculus in C57BL/6J and CBA/J mice across the life span. Neurobiol Aging. 1994; 15:175–83. [PubMed: 7838288]

Woodruff-Pak DS, Foy MR, Akopian GG, Lee KH, Zach J, Nguyen KP, Comalli DM, Kennard JA, Agelan A, Thompson RF. Differential effects and rates of normal aging in cerebellum and hippocampus. Proc Natl Acad Sci U S A. 2010; 107:1624–9. [PubMed: 20080589]

Yang DS, Kumar A, Stavrides P, Peterson J, Peterhoff CM, Pawlik M, Levy E, Cataldo AM, Nixon RA. Neuronal apoptosis and autophagy cross talk in aging PS/APP mice, a model of Alzheimer's disease. Am J Pathol. 2008; 173:665–81. [PubMed: 18688038]

Zettel ML, Frisina RD, Haider SE, O'Neill WE. Age-related changes in calbindin D-28k and calretinin immunoreactivity in the inferior colliculus of CBA/CaJ and C57Bl/6 mice. J Comp Neurol. 1997; 386:92–110. [PubMed: 9303527]

Zettel ML, Zhu X, O'Neill WE, Frisina RD. Age-related decline in Kv3.1b expression in the mouse auditory brainstem correlates with functional deficits in the medial olivocochlear efferent system. J Assoc Res Otolaryngol. 2007; 8:280–93. [PubMed: 17453307]

Zimniak P. Detoxification reactions: relevance to aging. Ageing Res Rev. 2008; 7:281–300. [PubMed: 18547875]

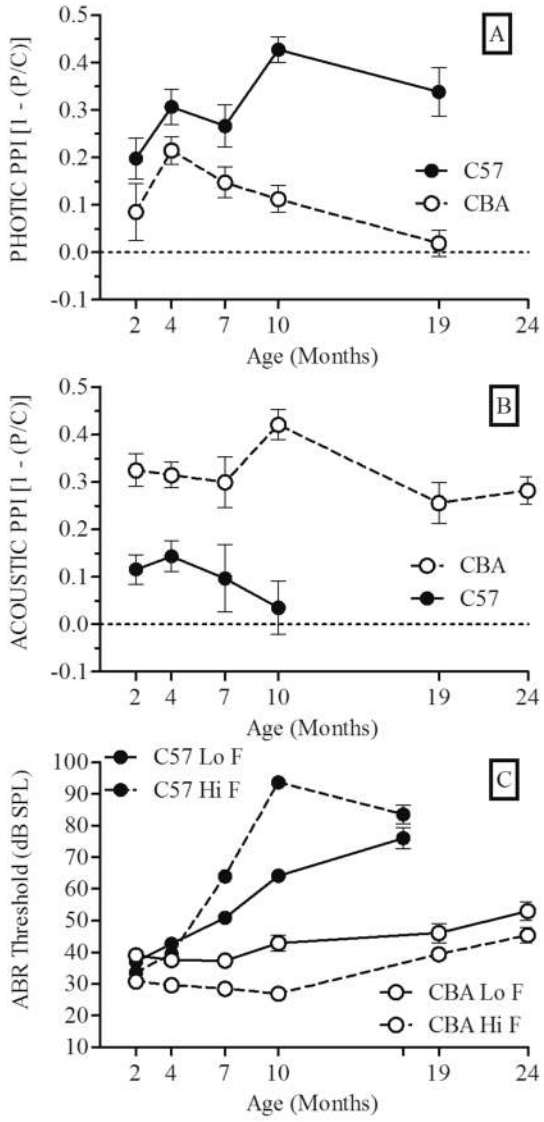

Figure 1.

Changes in sensitivity to acoustic and photic stimulation with increasing age in C57 and CBA mice. **A.** Mean (SEM) strength in reflex inhibition (PPI) provided by a light flash summed over 70, 110 and 160 ms before the startle noise burst. The difference in photic sensitivity between the two strains was minimal in young mice, but the two groups separated as performance steadily decreased in CBA mice between 4 and 19 months of age. **B.** Mean strength in reflex inhibition (PPI) provided by an acoustic stimulus, a brief gap in a background noise, summed over 60, 110 and 160 ms before the startle noise burst. The greater sensitivity of the CBA mice to this acoustic stimulus was present even in the youngest mice, then the difference between the groups increased with advancing age as performance decreased between 4 and 10 months of age in C57 mice. **C.** Age-related changes in hearing thresholds provided by the ABR technique. The test frequencies are grouped as low frequency, (Lo F, Mean SEM of 3 and 6 kHz) and high frequency (Hi F, Mean (SEM) of 24, 32, and 48 kHz). There was no significant difference between the strains at 2 months of age, but differences emerged within the first year of life, as thresholds for the C57 mice rapidly increased, especially at Hi F. By the end of the second year the thresholds

for the C57 mice were beyond the intensity limits of our instruments (> 90 dB SPL) while the thresholds for the CBA mice were minimally affected by just 10 to 15 dB.

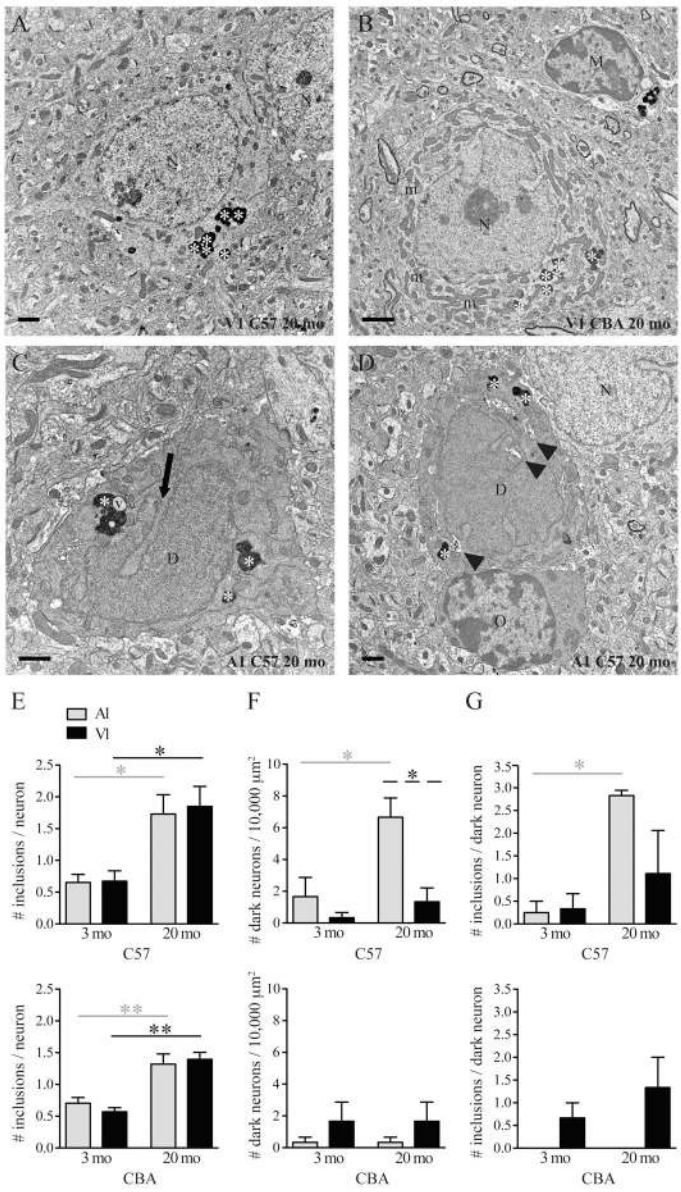

Figure 2.

Ultrastructural changes in neurons during normal aging and age-related sensory impairment in C57 and CBA mice. **A**–**D**: EM images showing aged neurons that contain multiple lysosomal inclusions (asterisks) and/or mitochondria in their perikaryal cytoplasm (m; **B**). In **C** and **D**, the neurons display condensed, electron-dense cytoplasm and nucleoplasm, more frequent ruffling of the plasma membrane, extensive invagination of the nuclear membrane (arrow; **C**), and dilation of the endoplasmic reticulum (arrowheads; **D**), possibly suggesting an ongoing degenerative process. D, dark neuron; M, microglia; N, neuron; O, oligodendrocyte. Scale bars=1 µm. **E**–**G**: Number of lysosomal inclusions per neuron (**E**), number of dark neurons per 10,000 μm^2 of ultrathin section (**F**), and number of lysosomal inclusions per dark neuron (**G**; mean ± SEM). Grey lines and asterisks refer to statistical comparisons between A1 regions, black lines and asterisks to comparisons between V1 regions, and black dotted line and asterisk to comparison between A1 and V1 regions. *, $p<0.05$ and **, $p<0.01$.

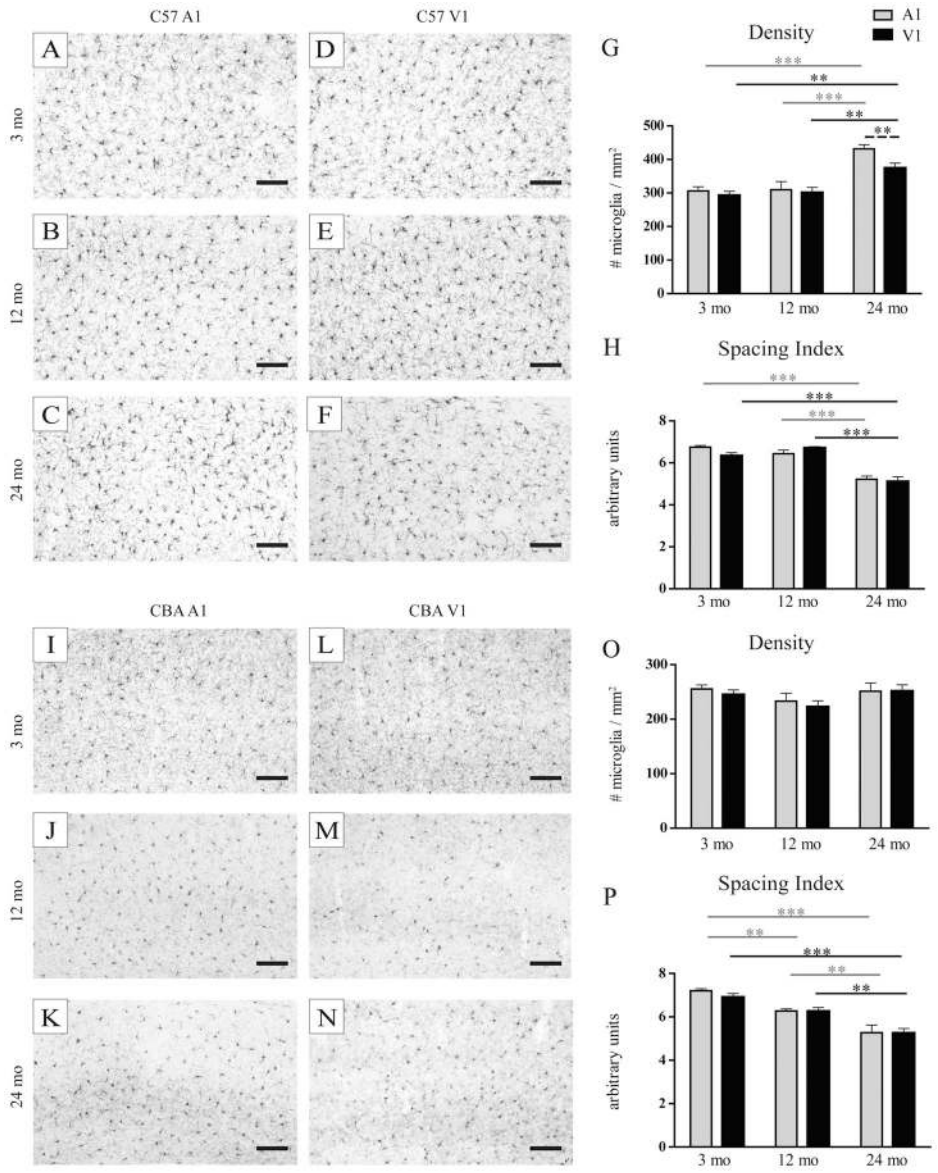

Figure 3.

Changes in density and distribution of microglia in C57 and CBA mice. **A–L**: low magnification photomicrographs showing an increase in density and clumping in C57 A1 **A–F, I–N**: low magnification photomicrographs showing an increase in density and clumping in A1 (**AC**) and V1 (**D–F**) of the C57 in contrast to an increase in clumping without change in density in A1 (**I–K**) and V1 (**L–N**) of the CBA. Scale bars=100 μm. Quantification of microglial density in C57 (**G**) and CBA (**O**), and spacing index in C57 (**H**) and CBA (**P**) mice. Statistics refer to *post hoc* analyses based on a 2-way ANOVA. **, p<0.01, ***, p<0.001. Statistical comparisons are illustrated as in Figure 2.

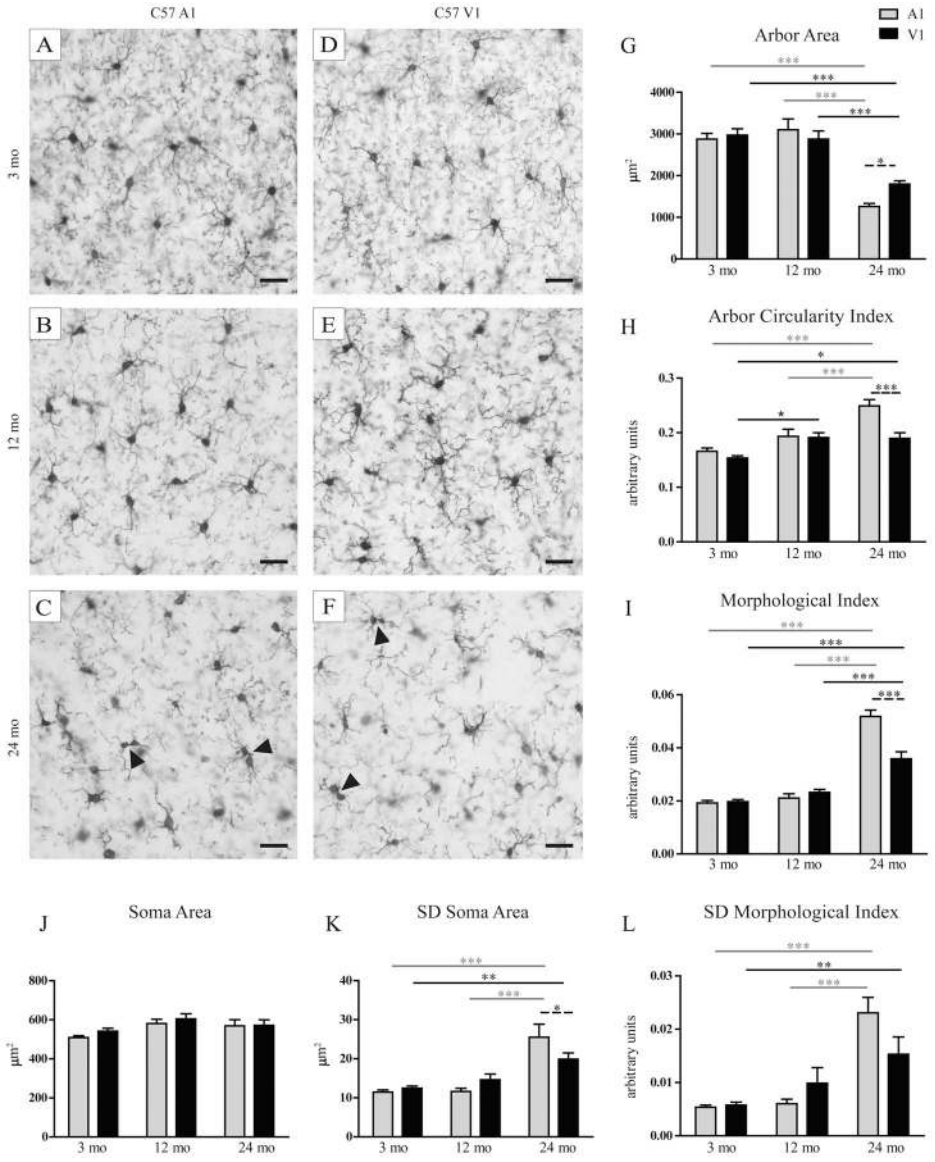

Figure 4.

Changes in the morphology of microglia in the C57 mouse. **A–F**: high magnification photomicrographs illustrating the decline in size and complexity of processes arborization without obvious changes in soma size in 24 mo C57 mice: A1 (**A–C**) and V1 (**D–F**). Scale bars=25 μm. Arrowheads show examples of clumped microglia. Quantification of the area of the process arbor (**G**), arbor circularity index (**H**), morphological index (**I**), average soma area (**J**), soma area standard deviation (SD; **K**), and morphological index standard deviation (**L**). Statistics refer to *post hoc* analyses based on a 2-way ANOVA. *, p< 0.05, **, p<0.01, ***, p<0.001. Statistical comparisons are illustrated as in Figure 2.

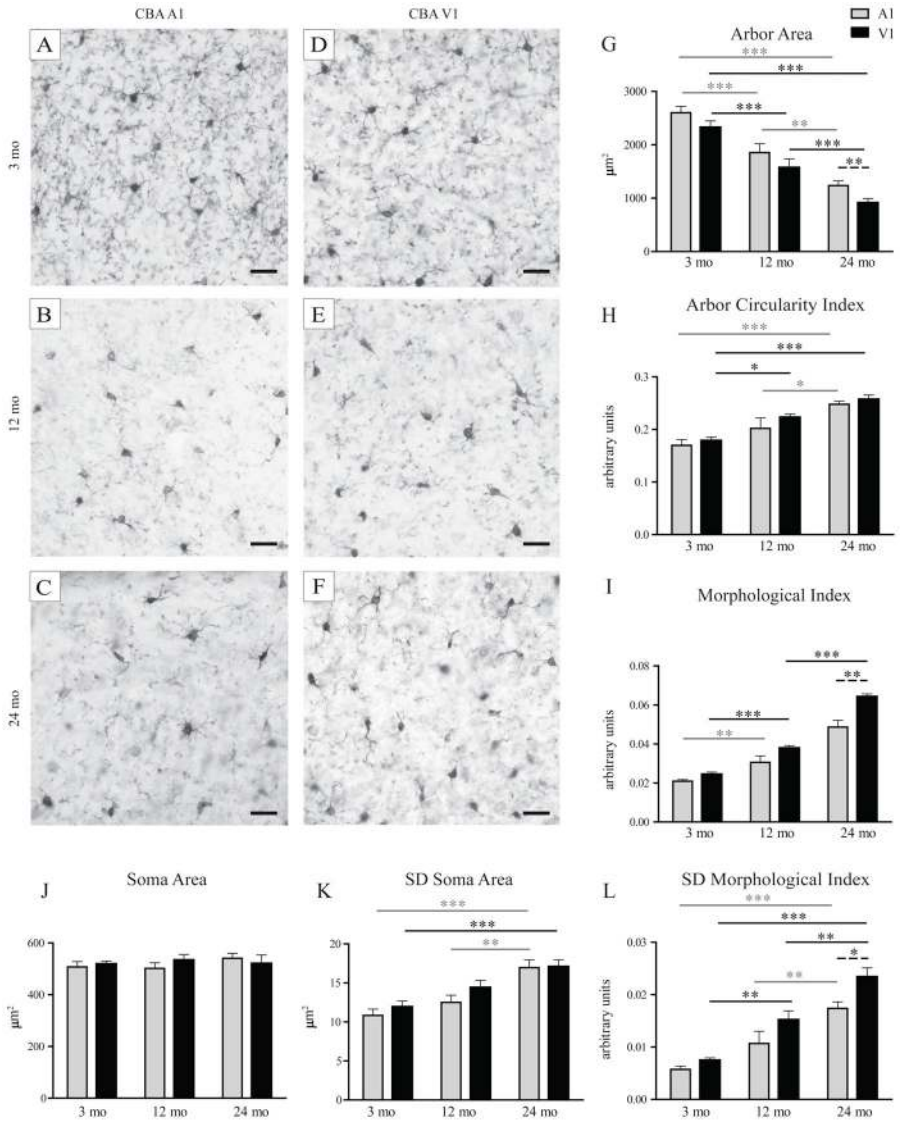

Figure 5.

Changes in the morphology of microglia in the CBA mouse. **A–F**: high magnification photomicrographs illustrating the decline in size and complexity of processes arborization without obvious changes in soma size by 12 mo in CBA mice: A1 (**A–C**) and V1 (**D–F**). Scale bars=25 μm. Quantification of the area of the process arbor (**G**), arbor circularity index (**H**), morphological index (**I**), average soma area (**J**), soma area standard deviation (SD; **K**), and morphological index standard deviation (**L**). Statistics refer to *post hoc* analyses based on a 2-way ANOVA. **, p<0.01, ***, p<0.001. Statistical comparisons are illustrated as in Figure 2.

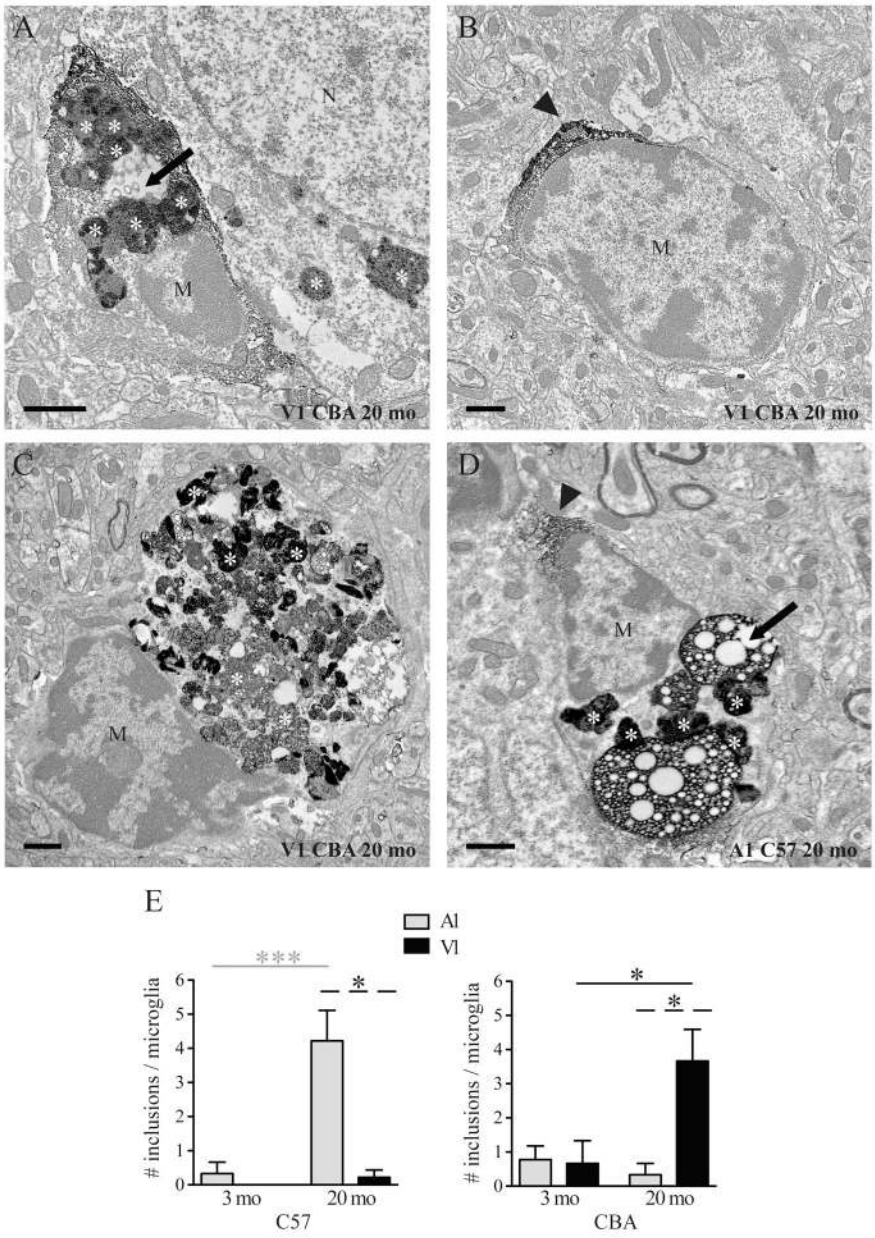

Figure 6.

Ultrastructural changes in microglia in C57 and CBA mice. **A**–**D**: Aged microglia accumulating various types of non-cellular inclusions, including lysosomal inclusions (asterisks), vacuoles and large vesicles (arrow; **A**), and lipid droplets of various sizes (arrow; **D**), which could result from the phagocytic elimination of neurons or glial cells. The microglia in **C** appears almost completely filled by cellular debris, akin to fat granule cells or *gitter* cells. Also note the size diversity of microglial cell bodies (see **A** and **D** for example of normal size, **B** and **C** for example of enlarged size). Immunoperoxidase staining for the microglia-specific marker IBA1 is shown by arrowheads. M, microglia. Scale bars=1 μm. **E**: Number of inclusions per microglia (lysosomal inclusions, vacuoles, small to large vesicles, lipid droplets, and cellular elements such as dendritic spines and axon terminals (see Figure 7); mean ± SEM). Statistical comparisons are illustrated as in Figure 2. *, $p<0.05$ and ***, $p<0.001$.

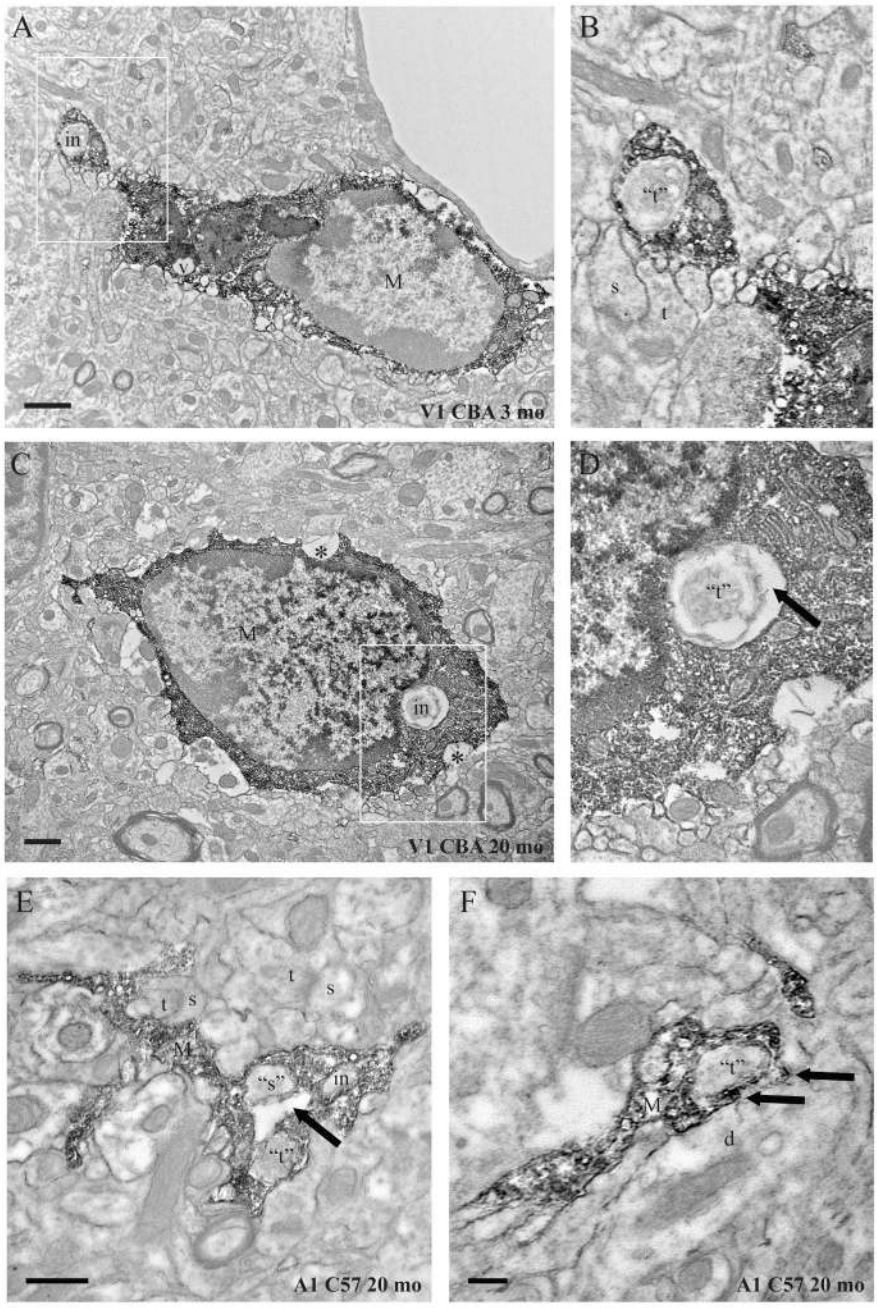

Figure 7.

Changes in microglial engulfment of synaptic elements in C57 and CBA mice. **A–F**: Young and aged microglia displaying cellular inclusions (in) in their cell body (**C**, inset in **D**), proximal process (**A**, inset in **B**), or distal processes (**E** and **F**). Cellular inclusions sometimes resembled profiles of axon terminals ("t"; see **B** and **D–F** for examples) and dendritic spines ("s"; **E** for example) with contained pockets of electron-lucent space (arrows; **D** and **E**), suggesting the phagocytic engulfment of synaptic elements by microglia. In **F**, the microglia extends a fine process (arrows) between an axon terminal that appears completely ensheathed ("t") and a dendrite (d), in a way reminiscent of synaptic stripping. In all pictures, microglial profiles show an electron-dense immunoperoxidase staining for

IBA1. M, microglia; s, dendritic spine; t, axon terminal; v, vacuole. Scale bars=1 μm for **A**–**D**, 0.5 μm for **E**, and 0.25 μm for **F**.

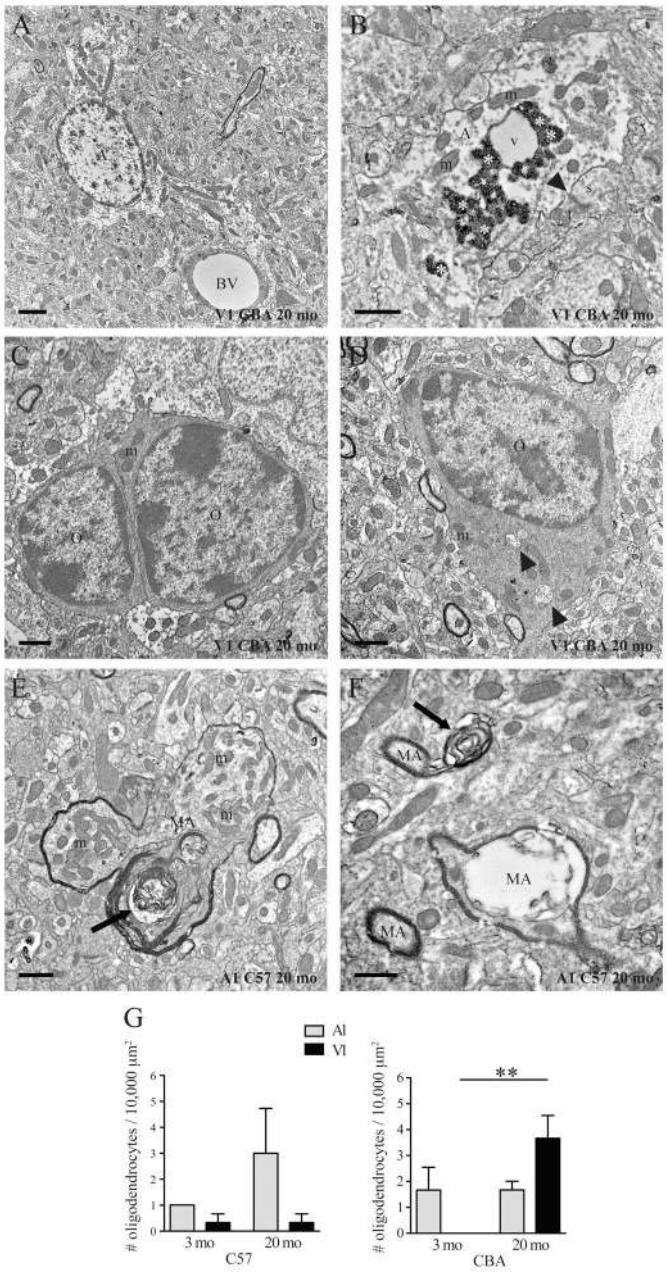

Figure 8.

Ultrastructural changes in astrocytes, oligodendrocytes, and axonal myelination in C57 and CBA mice. **A** and **B**: EM examples of aged astrocytes (**A**) with enlarged processes typically surrounding a blood vessel (BV; **A**) or containing large accumulations of lysosomal inclusions (**B**). **C** and **D**: Aged oligodendrocytes (O) devoid of lysosomal inclusions, encountered in a pair (**C**) or containing electron-lucent pockets in their perikaryal cytoplasm (arrowheads). **E** and **F**: Myelinated axons (MA) with redundant (arrows; **E** and **F**) or ballooned (see the large electron-lucent space in the sheath of the lower right MA; **F**) myelin sheaths. m, mitochondria. Scale bars=1 µm. G. Number of oligodendrocytes per 10,000 μm^2 of ultrathin section (mean ± SEM). Statistical comparisons are illustrated as in Figure 2. **, $p<0.01$.

Glia. Author manuscript; available in PMC 2013 April 1.

Table 1

EM quantification and statistics

			Mean ± SEM				2-way ANOVAs			
			3mo		20mo		Region		Age	
Cell type	**Measure**	**Strain**	**A1**	**V1**	**A1**	**V1**	**3 mo**	**20mo**	**A1**	**V1**
Neurons	Number	C57	30 ± 1	32 ± 4	29 ± 2	23 ± 3	NS	NS	NS	NS
		CBA	34 ± 8	28 ± 5	23 ± 4	24 ± 1	NS	NS	NS	NS
	Inclusions	C57	0.65 ± 0.1	0.67 ± 0.2	1.7 ± 0.3	1.8 ± 0.3	NS	NS	<0.05	<0.05
		CBA	0.71 ± 0.09	0.57 ± 0.06	1.3 ± 0.2	1.4 ± 0.1	NS	NS	<0.01	<0.01
Dark Neurons	Number	C57	1.7 ± 1	0.33 ± 0.3	6.7 ± 1	1.3 ± 0.9	NS	<0.05	<0.05	NS
		CBA	0.33 ± 0.3	1.7 ± 1	0.33 ± 0.3	1.7 ± 1	NS	NS	NS	NS
	Inclusions	C57	0.25 ± 0.3	0.33 ± 0.3	2.8 ± 0.1	1.1 ± 0.9	NS	NS	<0.05	NS
		CBA	0	0.67 ± 0.3	0	1.3 ± 0.7	NS	NS	NS	NS
Microglia	Number	C57	1.0 ± 0	3.3 ± 0.9	2.3 ± 0.7	2.3 ± 0.7	NS	<0.05	NS	<0.001
		CBA	1.0 ± 0.6	1.3 ± 0.3	1.0 ± 0	2.3 ± 0.3	NS	<0.05	NS	<0.05
	Inclusions	C57	0.33 ± 0.3	0	4.2 ± 0.9	0.22 ± 0.2	NS	<0.05	<0.001	NS
		CBA	0.78 ± 0.4	0.67 ± 0.7	0.33 ± 0.3	3.7 ± 0.9	NS	<0.05	NS	<0.05
Astrocytes	Number	C57	1.3 ± 0.3	2.0 ± 0.6	2.7 ± 0.9	2.0 ±1	NS	NS	NS	NS
		CBA	1.7 ± 0.3	2.0 ± 0.6	3.3 ± 0.3	2.3 ± 0.3	NS	NS	<0.05	NS
	Inclusions	C57	0	0	2.7 ± 2	0.42 ± 0.4	NS	NS	NS	NS
		CBA	0	0	0	0.33 ± 0.3	NS	NS	NS	NS
Oligodendrocytes	Number	C57	1.0 ± 0	0.33 ± 0.3	3.0 ± 2	0.33 ± 0.3	NS	NS	NS	NS
		CBA	1.7 ± 0.9	0	1.7 ± 0.3	3.7 ± 0.9	NS	NS	NS	<0.01
	Inclusions	C57	0	0.33 ± 0.3	0	0	NS	NS	NS	NS
		CBA	0.11 ± 0.1	0	0.17 ± 0.2	0.98 ± 0.2	NS	<0.05	NS	<0.01

Table 2

LM quantification and statistics

		2-way ANOVAs		Mean ± SEM					
		Region	Age	3 mo		12 mo		24 mo	
Measure	strain			A1	V1	A1	V1	A1	V1
Density	C57	< .01	<.0001	177 ± 7.2	169 ± 7.0	179 ± 14.0	174 ± 9.0	249 ± 7.2	216 ± 8.5
	CBA	NS	NS	148 ± 4.3	142 ± 4.8	135 ± 8.4	129 ± 6.4	145± 8.6	146 ± 6.6
Spacing Index	C57	NS	<.0001	6.7 ± .086	6.3 ± .15	6.4 ± .17	6.7 ± .07	5.2 ±.15	5.1 ± .24
	CBA	NS	<.0001	7.2 ± .088	6.9 ± .163	6.3 ± .097	6.3 ± .169	5.3 ± .352	5.2 ± .214
Arbor Area	C57	< .05	<.0001	27993 ± 1324	28915 ± 1491	30166 ± 2536	27971 ± 1919	12243 ± 715	17468 ± 786
	CBA	< .01	<.0001	25333 ± 1121	22613 ± 1202	18043 ± 1601	15289 ± 397	12040 ± 878	8871 ± 807
MI	C57	p< .05	<.0001	0.019 ± .0009	0.02 ± .0008	0.021 ± .0017	0.023 ± .001	0.052 ± .002	0.036 ± .003
	CBA	<.001	<.0001	0.021 ± .0009	0.024 ± .0012	0.031 ± .0033	0.038 ± .0014	0.049 ± .0034	0.064 ±.0015
MI SD	C57	NS	<.0001	0.005 ± .0004	0.006 ± .0006	0.006 ± .0008	0.01 ± .0029	0.023 ± .0029	0.015 ±.0032
	CBA	p< .05	<.0001	0.006 ± .0006	0.007 ± .0005	0.011 ± .0023	0.015 ± .0017	0.017 ± .0012	0.023 ± .0017
Arbor Circularity	C57	< .01	<.0001	0.166 ± .006	0.154 ± .004	0.193 ± .013	0.191 ± .009	0.25 ± .011	0.19 ± .010
	CBA	NS	<.0005	0.17 ± .011	0.179 ± .007	0.202 ± .020	0.223 ± .006	0.248 ± .006	0.257 ± .008
Soma Area	C57	NS	NS	509 ± 9.08	542 ± 15.35	581 ± 22.46	605 ± 25.69	569 ± 31.31	571 ± 27.99
	CBA	NS	NS	507 ± 20.85	519 ± 10.97	502 ± 21.56	533 ± 21.55	541 ± 19.26	520 ± 33.23
Soma Area SD	C57	p< .05	<.0001	111 ± 5.35	121 ± 5.58	113 ± 7.95	142 ± 14.30	248 ± 32.42	194± 15.52
	CBA	NS	<.0001	106 ± 7.86	116 ± 7.34	122 ± 8.90	140 ± 8.91	165± 10.04	166 ± 8.67